

Magnetic loss, permeability, and anisotropy compensation in CoO-doped Mn-Zn ferrites

*Original*

Magnetic loss, permeability, and anisotropy compensation in CoO-doped Mn-Zn ferrites / Beatrice, Cinzia; Dobák, Samuel; Tsakaloudi, Vasiliki; Ragusa, Carlo; Fiorillo, Fausto; Martino, Luca; Zaspalis, Vassilis. - In: AIP ADVANCES. - ISSN 2158-3226. - ELETTRONICO. - 8:4(2018), p. 047803. [10.1063/1.4993718]

*Availability:*

This version is available at: 11583/2700117 since: 2018-02-28T17:18:54Z

*Publisher:*

American Institute of Physics Inc.

*Published*

DOI:10.1063/1.4993718

*Terms of use:*

This article is made available under terms and conditions as specified in the corresponding bibliographic description in the repository

*Publisher copyright*

(Article begins on next page)

## Magnetic loss, permeability, and anisotropy compensation in CoO-doped Mn-Zn ferrites

Cinzia Beatrice, Samuel Dobák, Vasiliki Tsakaloudi, Carlo Ragusa, Fausto Fiorillo, Luca Martino, and Vassilis Zaspalis

Citation: [AIP Advances](#) **8**, 047803 (2018); doi: 10.1063/1.4993718

View online: <https://doi.org/10.1063/1.4993718>

View Table of Contents: <http://aip.scitation.org/toc/adv/8/4>

Published by the [American Institute of Physics](#)

---

### Articles you may be interested in

[Improving soft magnetic properties of Mn-Zn ferrite by rare earth ions doping](#)

[AIP Advances](#) **8**, 047807 (2018); 10.1063/1.4993645

[Frequency dispersion of complex permeability in Mn-Zn and Ni-Zn spinel ferrites and their composite materials](#)

[Journal of Applied Physics](#) **93**, 2789 (2003); 10.1063/1.1542651

[Mg<sub>1-x</sub>Zn<sub>x</sub>Fe<sub>2</sub>O<sub>4</sub> nanoparticles: Interplay between cation distribution and magnetic properties](#)

[AIP Advances](#) **8**, 047804 (2018); 10.1063/1.4994015

[Effect of lanthanum substitution on structural and magnetic properties of nickel zinc ferrites](#)

[AIP Advances](#) **8**, 047802 (2018); 10.1063/1.4993530

[Study of magnetic properties of NiZnCu ferrite synthesized by Pechini method and solid-state reactions](#)

[AIP Advances](#) **8**, 047801 (2018); 10.1063/1.4994035

[Decomposing the permeability spectra of nanocrystalline finemet core](#)

[AIP Advances](#) **8**, 047205 (2018); 10.1063/1.4991941

---



**Don't** let your writing  
keep you from getting  
published!

**AIP** | Author Services

Learn more today!

## Magnetic loss, permeability, and anisotropy compensation in CoO-doped Mn-Zn ferrites

Cinzia Beatrice,<sup>1,a</sup> Samuel Dobák,<sup>2,b</sup> Vasiliki Tsakaloudi,<sup>3</sup> Carlo Ragusa,<sup>4</sup> Fausto Fiorillo,<sup>1</sup> Luca Martino,<sup>1</sup> and Vassilis Zaspalis<sup>5</sup>

<sup>1</sup>Nanoscience and Materials Department, Istituto Nazionale di Ricerca Metrologica INRIM, 10135 Torino, Italy

<sup>2</sup>Institute of Physics, P.J. Šafárik University, 04022 Košice, Slovakia

<sup>3</sup>Laboratory of Inorganic Materials, CERTH, 57001 Thessaloniki, Greece

<sup>4</sup>Energy Department, Politecnico di Torino, 10129 Torino, Italy

<sup>5</sup>Department of Chemical Engineering, Aristotle University of Thessaloniki, 54124 Thessaloniki, Greece

(Received 30 June 2017; accepted 8 September 2017; published online 17 October 2017)

Mn-Zn ferrite samples prepared by conventional solid state reaction method and sintering at 1325 °C were Co-enriched by addition of CoO up to 6000 ppm and characterized versus frequency (DC – 1GHz), peak polarization (2 mT – 200 mT), and temperature (23 °C – 120 °C). The magnetic losses at room temperature are observed to pass through a deep minimum value around 4000 ppm CoO at all polarizations values. This trend is smoothed out either by approaching the MHz range or by increasing the temperature. Conversely, the initial permeability attains its maximum value around the same CoO content, while showing moderate monotonical decrease with increasing CoO at the typical working temperatures of 80 – 100 °C. The energy losses, measured by a combination of fluxmetric and transmission line methods, are affected by the eddy currents, on the conventional 5 mm thick ring samples, only beyond a few MHz. Their assessment relies on the separation of rotational and domain wall processes, which can be done by analysis of the complex permeability and its frequency behavior. This permits one, in particular, to calculate the magnetic anisotropy and its dependence on CoO content and temperature and bring to light its decomposition into the host lattice and Co<sup>2+</sup> temperature dependent contributions. The temperature and doping dependence of initial permeability and magnetic losses can in this way be qualitatively justified, without invoking the passage through zero value of the effective anisotropy constant upon doping. © 2017 Author(s). All article content, except where otherwise noted, is licensed under a Creative Commons Attribution (CC BY) license (<http://creativecommons.org/licenses/by/4.0/>). <https://doi.org/10.1063/1.4993718>

### I. INTRODUCTION

The introduction of additional oxides is the classical strategy adopted for improving the broad-band soft magnetic properties of Mn-Zn ferrites. One aims in this way at reduced eddy current losses, increased frequency stability of the permeability and optimal response at the typical working temperatures of the device cores.<sup>1,2</sup> The main physical mechanisms by which the dopants can affect the ferrite magnetic properties consist either in the segregation of the foreign species at the grain boundaries or their dissolution inside the grains, thereby modifying the resistivity, the intrinsic magnetic properties, and possibly the microstructure of the material.<sup>3–5</sup> It is thus standard practice, for example, to introduce CaO and Nb<sub>2</sub>O<sub>5</sub> in order to modify the chemistry at the grain boundaries and increase the related resistivity, an effect that can be reinforced by adding SiO<sub>2</sub> or Ta<sub>2</sub>O<sub>5</sub>.<sup>6,7</sup> At the same time,

<sup>a</sup>Author to whom correspondence should be addressed. [c.beatrice@inrim.it](mailto:c.beatrice@inrim.it).

<sup>b</sup>This research was performed while S. Dobák was at the Nanoscience and Materials Department of INRIM, Torino, Italy.

with additives like  $\text{TiO}_2$ ,  $\text{SnO}_2$ , and  $\text{CoO}$  and the corresponding substitution of  $\text{Fe}^{3+}$  cations with the foreign cations, the mechanism of hopping conduction between  $\text{Fe}^{2+}$ -  $\text{Fe}^{3+}$  ions can be hindered and the intragrain resistivity can increase.<sup>3,8-10</sup> In addition, the phenomenon of anisotropy compensation, where the negative anisotropy of the  $\text{Fe}^{3+}$  ions in the octahedral sites is made to combine with the positive anisotropy of the extra-cations occupying the same sites, is expected to occur, thereby lowering, in a temperature-dependent fashion, the overall magnetocrystalline anisotropy.<sup>11</sup> Standard Mn-Zn ferrites generally rely on anisotropy compensation by extra  $\text{Fe}^{2+}$  ions, an effect that can be modulated by the additives, eventually affecting to large extent energy loss and permeability at all temperatures. These concepts are relatively well understood at a qualitative level, but hard to translate into a quantitative assessment, because this would require precise description of the magnetization process and the mechanisms of magnetic energy losses. The very low values of the anisotropy constant attained in these materials can indeed strongly enhance the rotational processes, if compared with the conventional steel sheets. On the other hand, the semi-insulating character of these materials naturally leads, depending on sample size and magnetizing frequency, to consider the dissipation channel associated with spin damping.

In this work we have investigated the effect of  $\text{CoO}$  doping on the properties of Mn-Zn sintered ferrites and developed a method to recognize the ensuing evolution of the permeability and energy loss behavior in terms of anisotropy evolution. This method takes at face value the broadband frequency response of the material by modeling the frequency dependence of permeability and losses and separating the contributions to the magnetization process of domain wall (dw) displacements and rotations. Rotation modeling is based, in turn, on the solution of Landau-Lifshitz equation and averaging under assumed distribution of the local (at the scale of the single grain) anisotropies. With the DC rotational susceptibility connected, for a uniform orientation distribution of the easy axes, to the average anisotropy  $K$  as  $\chi_{\text{DC,rot}} = J_s^2/3\mu_0|K|$ , we eventually obtain, knowing the dependence of the saturation polarization  $J_s$  on  $\text{CoO}$  content  $c_{\text{Co}}$  ( $0 \leq c_{\text{Co}} \leq 6000$  ppm) and temperature  $T$ , the dependence of the effective anisotropy constant on  $c_{\text{Co}}$  and  $T$ . By denoting  $K$  as effective, we take into account that the torque involved with rotational processes involves both magnetocrystalline and local magnetostatic effects. It is thus verified that the calculated  $K(c_{\text{Co}})$  is minimum for  $c_{\text{Co}} = 3000 - 4000$  ppm, corresponding to minimum magnetic losses and maximum initial permeability.  $K(c_{\text{Co}}, T)$  shows a monotonical decrease with increasing temperature. The secondary maximum of the initial permeability, observed around  $T = 90^\circ\text{C}$ , turns then out to be related, according to the previous expression for  $\chi_{\text{DC,rot}}$ , to the competition between the decreasing behaviors of  $J_s$  and  $K$  with the temperature. In any case, the estimated anisotropy contribution by the  $\text{Co}^{2+}$  cations  $K_{\text{Co}}(T) = K(c_{\text{Co}}, T) - K(c_{\text{Co}}=0, T)$  appears to engender a decrease of  $K(T)$  below about  $60^\circ\text{C}$  only for  $c_{\text{Co}} < 5000$  ppm.

## II. SAMPLE PREPARATION. STRUCTURAL, ELECTRICAL, AND MAGNETIC CHARACTERIZATION

Mn-Zn ferrite powders were prepared following the conventional method of solid state reaction, starting from high-purity raw materials. Dry mixing of the Fe, Mn, and Zn oxides was performed using a laboratory mixer and prefiring took place at  $850^\circ\text{C}$  in air. The resulting powders had the proportions:  $\text{Fe}_2\text{O}_3 = 72$  wt%,  $\text{MnO} = 21.60$  wt%,  $\text{ZnO} = 6.35$ wt %. The prefired powders were doped with a fixed doping scheme that included  $\text{CaO}$  and  $\text{Nb}_2\text{O}_5$ , while Co doping varied between 0-6000 ppm of  $\text{CoO}$ , step 1000. After milling, roll granulation was performed using a rotating drum with the addition of 0.2 wt% of aqueous solution of polyvinyl alcohol (Merck, Analytical Grade, MW72000). Specimens of toroidal shape of outside diameter of 14 mm were uniaxially pressed to a press density of  $2.90 \text{ g/cm}^3$  and sintered at a top temperature of  $1325^\circ\text{C}$  under controlled partial oxygen pressure, according to the Morineau-Paulus equilibrium condition. The sinter density of the Mn-Zn ferrites was measured by the Archimedes' method. The polycrystalline microstructure of the sintered specimens was investigated By Scanning Electron Microscopy (JEOL 6300), after grinding, polishing and chemical etching of the sintered ferrites. The X-Ray Diffraction analysis showed that in all the prefired powders the initial spinel structure was successfully formed. As shown in Table I, the sinter density of the compacted and sintered toroidal specimens, measured by Archimedes's method, was observed to increase slightly with  $\text{CoO}$  doping, up to 2.4 % with  $\text{CoO} = 6000$  ppm.

TABLE I. Physical parameters of the investigated CoO-doped Mn-Zn ferrites.

Sample	CoO (ppm)	Grain size $\langle s \rangle$ ( $\mu\text{m}$ )	Density $\delta$ ( $\text{kg/m}^3$ )	DC resistivity $\rho_{\text{DC}}$ ( $\Omega\text{ m}$ )	Real resistivity at 10 MHz $\rho'_{10\text{MHz}}$ ( $\Omega\text{ m}$ )	Imaginary resistivity at 10 MHz $\rho''_{10\text{MHz}}$ ( $\Omega\text{ m}$ )
A0	0	10.8	4.92	4.42	0.0130	-0.0076
A1	1000	10.7	4.98	5.08	0.0170	-0.0080
A2	2000	11.9	4.98	5.39	0.0165	-0.0073
A3	3000	12.2	5.01	5.52	0.0195	-0.0069
A4	4000	13.1	4.98	5.66	0.0185	-0.0069
A5	5000	10.8	5.01	5.9	0.0154	-0.0076
A6	6000	11.1	5.04	6.1	0.0137	-0.0096

The micrographs obtained by SEM-Jeol 6300 images of the polished and etched sample surface showed little variation of the average grain size, which attained a maximum value of 13.1  $\mu\text{m}$  for CoO = 4000 ppm (see Table I and Fig. 1).

The electrical impedance was measured from DC to 20 MHz by means of a standard four-wire method, with good voltmetric and amperometric electrical contacts ensured by indium strips sandwiched, at the ends of a cut ring sample, between the polished sample surface and copper leads subjected to uniform pressure. The measuring method and a general discussion of the frequency dependence of the complex resistivity  $\rho(f) = \rho'(f) + j\rho''(f)$  in typical ferrites are illustrated in Ref. 12. It is found in the present case that the real part  $\rho'$  of the resistivity exhibits the usual double-plateau dependence on frequency,<sup>12</sup> with the DC value  $\rho_{\text{DC}}$  monotonically increasing from 4.42  $\Omega\text{m}$  to 6.1  $\Omega\text{m}$  on passing from the undoped to the 6000 ppm CoO doped ferrite and the high-frequency plateau (observed beyond about  $f = 1$  MHz) attaining a value around 0.015 – 0.020  $\Omega\text{m}$ . The imaginary part  $\rho''$  displays the well known capacitive character, as dictated by the thin insulating grain boundary.<sup>12</sup> The DC resistivity  $\rho_{\text{DC}}$  is thus overwhelmingly associated with the grain boundaries, which are capacitively short-circuited at high frequencies, so that the high-frequency resistivity basically coincides with the grain resistivity. The evolution of DC resistivity and the real and imaginary resistivities at 10 MHz versus CoO doping is shown in Table I.

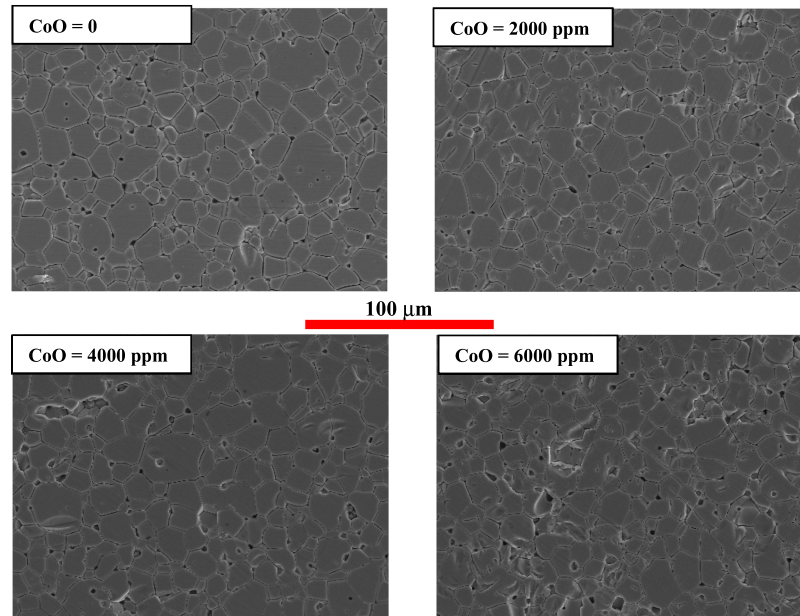


FIG. 1. SEM micrographs of the sintered Mn-Zn ferrites (sintering temperature  $T = 1325^\circ\text{C}$ ) with different CoO contents. The average grain size is little affected by addition of CoO (see Table I).

TABLE II. Selected magnetic parameters in the Mn-Zn ferrites versus CoO content at room temperature.  $J_s$   $\equiv$  saturation polarization;  $\mu_{r,2mT}$   $\equiv$  initial permeability at 100 kHz;  $\mu'_{r,100mT}$   $\equiv$  real permeability at 100 mT and 100 kHz;  $W_{100mT}$   $\equiv$  Energy loss at 100 mT and 100 kHz;  $\mu_{DC,rot}$   $\equiv$  DC rotational permeability;  $K$   $\equiv$  calculated average anisotropy constant.

Sample	CoO (ppm)	$J_s$ (T)	$\mu_{r,2mT}$	$\mu'_{r,100mT}$	$W_{100mT}(\text{J/m}^3)$	$\mu_{DC,rot}$	$K$ (J/m <sup>3</sup> )
A0	0	0.540	2230	4199	1.540	2110	36.68
A1	1000	0.534	2258	3889	1.310	2070	36.56
A2	2000	0.529	2480	3906	1.020	2210	33.61
A3	3000	0.524	2690	3742	0.845	2380	30.38
A4	4000	0.522	2555	3401	0.687	2300	31.44
A5	5000	0.532	2070	3712	1.185	1713	43.85
A6	6000	0.536	1385	3100	2.100	1190	64.07

The magnetic characterization of the sintered ring samples (outside diameter 14.15-14.44 mm, inside diameter 9.15 – 8.86 mm, thickness 4.55 – 5.02 mm) was performed by means of a calibrated hysteresigraph-wattmeter from DC to a maximum frequency of 10 MHz and from a few hundred kHz to 1 GHz by a transmission line method using a Vector Network Analyzer (VNA, Agilent 8753E, 10 mW irradiated power) and a 50  $\Omega$  coaxial line. The ring sample was placed against the shorted bottom of a clean 50  $\Omega$  brass cell and the complex permeability was obtained from the measurement of the scattering parameter in reflection. The fluxmetric and transmission line methods provided overlapping results in the common frequency interval. The measuring method, setup, and procedure are discussed in detail in Refs. 13,14. Measurements as function of temperature could also be performed up to 120 °C, as discussed in Ref. 15. The saturation polarization  $J_s$  as a function of temperature was in particular obtained. Table II summarizes the behavior of significant magnetic parameters as a function of CoO content. It is noted in Tables I and II and shown in Fig. 2 that the saturation polarization  $J_s$  and the grain resistivity (i.e.  $\rho'$  at 10 MHz) concurrently pass through maximum and minimum values value for a CoO content  $c_{Co} = 3000 - 4000$  ppm. The increase of the grain resistivity with the introduction of the CoO is consistent with the idea that the  $\text{Co}^{2+}$  cations entering the host lattice prevalently occupy the octahedral sites and take the place of either  $\text{Fe}^{2+}$  or  $\text{Fe}^{3+}$  ions (which are endowed with higher magnetic moment), thereby hindering electron hopping between  $\text{Fe}^{2+}$  and  $\text{Fe}^{3+}$  ions.<sup>8,9</sup> It appears, however, that this actually would occur only for  $c_{Co} < 4000$  ppm, because  $\rho'$  is observed to decrease again at high CoO contents, in association with an increase of  $J_s$ . The DC resistivity is instead observed to always increase with  $c_{Co}$ , pointing to correspondingly increasing dopant segregation at the grain boundaries. There is no unambiguous explanation for the

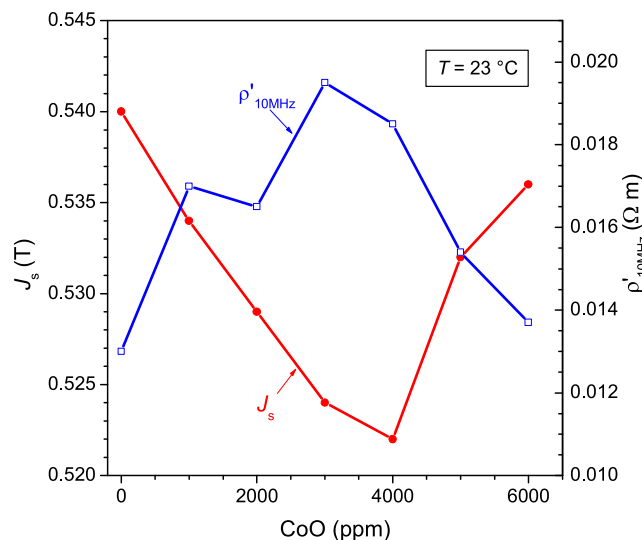


FIG. 2. Saturation polarization and real resistivity component at 10 MHz as a function of CoO content.

concurrent behaviors of grain resistivity and saturation polarization at the highest  $c_{\text{Co}}$  values. These could be possibly due to some kind of sharing of the Fe and Co cations between octahedral and tetrahedral sites. In any case, by adding dopants, like CoO, soluble in the spinel lattice, anisotropy compensation expectedly occurs. Indirect evidence for it is given by the evolution of initial permeability and magnetic losses with dopant content and temperature  $T$ .<sup>8–11</sup> This effect is well known and discussed in the literature, but no direct determination of the anisotropy evolution is provided.<sup>16</sup> We shall see in the following that, starting from analysis and modeling of the frequency dependence of permeability and losses, we are eventually able to describe the evolution of the anisotropy constant  $K$  with  $c_{\text{Co}}$  and  $T$ , and to single out the contributions from the host lattice and from the doping ions.

### III. PERMEABILITY, MAGNETIC LOSSES, AND THEIR ANALYSIS. ROLE OF DOPANT CONTENTS AND TEMPERATURE

A main aspect of the Mn-Zn ferrite phenomenology is represented by the loss and permeability response of the material as a function of the magnetizing frequency. One chief objective of ferrite development is then one of broadening, within the constraints given by the Snoek's law, the useful frequency band and of minimizing the energy losses at the typical working temperatures.<sup>7</sup> The strategy based on doping aims, besides the increase of the grain boundary resistivity, at modulating the magnetocrystalline anisotropy and its dependence on temperature, with ensuing effects on loss and permeability. The mechanism of anisotropy compensation is, in particular, expected to operate with  $\text{Co}^{2+}$  ions, but no quantitative information on the anisotropy behavior is so far available.

#### A. Magnetic permeability and losses. Rotations versus domain wall displacements

Our experimental approach relies first on a complete determination of complex permeability  $\mu = \mu' - j\mu''$  and energy loss  $W$ , up to the frequencies at which both  $\mu'$  and  $\mu''$  become vanishingly small. Fig. 3 provides an example (A2 sample,  $\text{CoO} = 2000$  ppm) of real permeability behavior measured up to 1 GHz for peak polarization value  $J_p$  ranging between 2 mT and 200 mT.

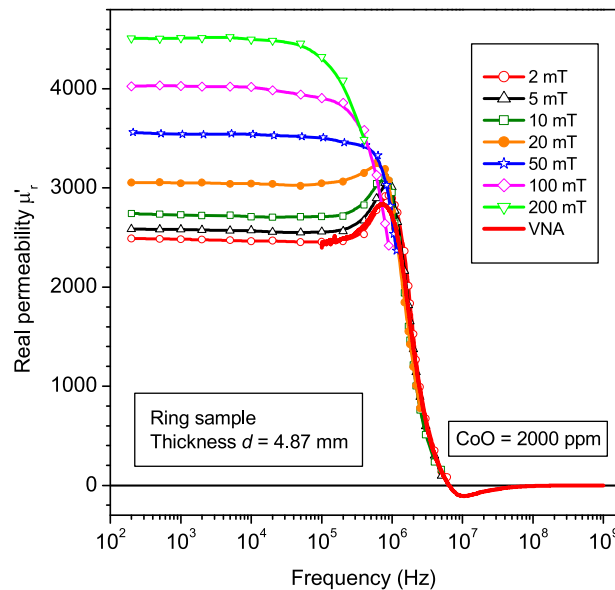


FIG. 3. Relative real permeability component  $\mu'_r$  versus frequency at given peak polarization values  $J_p = 2 - 200$  mT in the 2000 ppm CoO doped Mn-Zn ferrite sample. The fluxmetric measurements (open symbols) are performed up to the maximum frequency  $f = 10$  MHz. The result of the transmission line measurement (Vector Network Analyser (VNA) at 10 mW) is shown by the continuous line.



As discussed in previous papers<sup>12,17,18</sup> and shown in this figure, the VNA measurements, though performed under defined power (10 mW), overlap with the fluxmetric measurements made at different  $J_p$  values at sufficiently high frequencies. This fact is explained in terms of full relaxation of dw processes and uniquely surviving rotational processes at such frequencies.<sup>18</sup> It is also noted that  $\mu'$  is basically constant up to about 100 kHz, with resonant hump and relaxation decay occurring in the MHz region. The energy losses at given  $J_p$  value are fluxmetrically measured up to 10 MHz. They are instead calculated, when adopting the VNA method, from the measured complex permeability, according to

$$W(J_p, f) = \pi J_p^2 \frac{\mu''(f)}{\mu'^2(f) + \mu''^2(f)}. \quad (1)$$

Fig. 4 shows overlapping of the fluxmetric (symbols) and VNA (continuous lines) energy loss results, paralleling the permeability overlap observed in Fig. 3. On increasing the  $J_p$  value, the width of the overlapping frequency interval decreases, because the dw displacements increase their contribution, at the expenses of rotations. Practical measuring limitations do not permit one to fluxmetrically attain the MHz range beyond some 50 mT, but reasonable extrapolation to the high frequency VNA loss values can be made (short-dash lines in Fig. 4). By the VNA measurements, where the exciting field amplitude decreases with frequency, we almost exclusively excite the rotational processes. Branching of the VNA and fluxmetric loss curves (shown, for example, in Fig. 4 for  $J_p = 50, 100$ , and 200 mT between 100 kHz and 1 MHz) provides experimental evidence of the respective role played by the dw and the rotational losses. The shown  $W(f)$  curves refer to the as-obtained materials. By repeating the measurements after grinding the ring samples down to about 1 mm thickness, we conclude, according to the example shown for  $J_p = 10$  mT in Fig. 4, that the eddy currents can contribute to the energy loss, by an amount of the order of 10 - 20 %, only beyond a few MHz, in close analogy with previous experiments performed on Mn-Zn ferrites of different tickness.<sup>18</sup>

It has been shown in previous papers that the whole phenomenology of permeability and losses in Mn-Zn ferrites can be assessed to very good extent by detailed analysis and modeling of the

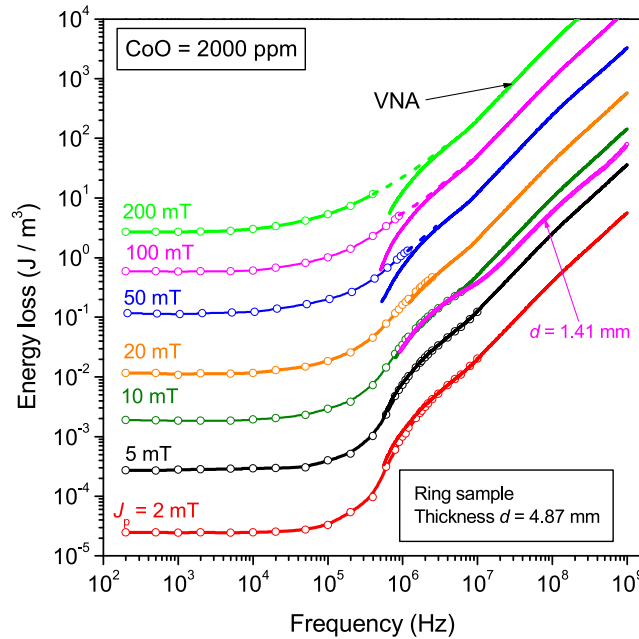


FIG. 4. Magnetic energy loss versus frequency at given peak polarization value  $J_p = 2 - 200$  mT (same sample as in Fig. 2). The energy loss in the VNA-covered high-frequency range (continuous lines) is obtained from the measured complex permeability by Eq. (1). The short-dashed lines provide extrapolation to high frequencies of the fluxmetric measurements made beyond  $J_p = 50$  mT. The measurement performed on a thinned (from  $d = 4.87$  mm to  $d = 1.41$  mm) ring sample shows that the eddy currents do contribute to the magnetic losses only at very high frequencies, above about 6 MHz.



magnetization process and the related dissipation mechanisms.<sup>12,17,18</sup> A fundamental approximation of modeling consists in separating the contributions of dw displacements and rotations, generalizing to poorly conducting materials the basic assumptions of the statistical theory of losses.<sup>19</sup> The rotations now parallel the mechanisms underlying the classical losses in magnetic sheets, while the local character of the dissipation by the dw's, whose dynamics can be described by the very same equations in conductive and in insulating magnetic materials,<sup>20</sup> is at the root of the hysteresis and excess losses. A procedure for enucleating dw and rotational permeabilities from the measured permeability versus frequency behavior can actually be worked out by a self-consistent procedure. This important aspect of the magnetization process is discussed in detail in Ref. 18. The method exploits the fact that the imaginary permeability at low-frequencies is exclusively associated with the dw processes  $\mu''_{DC} \equiv \mu''_{DC,dw}$ . On the other hand, the rotational permeability can be considered, for an assumed isotropic distribution of easy axes, quite independent of  $J_p$ , at least up to  $J_p \sim 0.1 J_s - 0.2 J_s$ . It is thus demonstrated in Ref. 18 that these two assumptions suffice to separately calculate  $\mu'_{dw}(J_p, f)$ ,  $\mu'_{rot}(J_p, f)$ ,  $\mu'_{rot}(f)$ , and  $\mu''_{rot}(f)$ . Figs. 5a and 5b provide an example, concerning the A4 sample (CoO = 4000 ppm), of permeability decomposition versus frequency. It is observed here that the initial permeability (the one measured, in our case, with  $J_p = 2$  mT) is overwhelmingly due to the rotational processes. The  $J_p$ -independent  $\mu'_{rot}(f)$ , and  $\mu''_{rot}(f)$  curves exhibit the expected resonant behavior, in contrast with the relaxation character of  $\mu'_{dw}(J_p, f)$  and  $\mu''_{dw}(J_p, f)$ . The overall dependence of the measured DC-permeability  $\mu_{DC}$  on the CoO content in the  $J_p$  interval 2 mT - 200 mT is shown in Fig. 6. The singled out rotational contribution  $\mu_{DC,rot}$  is observed to pass through a maximum value for CoO = 3000 – 4000 ppm. A more or less monotonical decrease of  $\mu_{DC}$  with CoO content is observed beyond about  $J_p = 50$  mT, where the dw contribution becomes prevalent. To note the small difference, consistent with the results shown in Fig. 5a, between  $\mu_{DC}$  and  $\mu'(100 \text{ kHz})$ . Fig. 6b shows that a greater stability of the initial permeability versus temperature is obtained for CoO = 3000 – 4000 ppm.

The dependence of permeability on  $c_{Co}$  shown in Fig. 6 is paralleled by the behavior of the energy loss  $W(f, J_p)$  shown in Fig. 7. This example refers to  $J_p = 100$  mT and the frequency range 100 Hz - 800 kHz. The softening role of CoO addition is apparent up to about 4000 ppm, where  $W(f)$  and  $\mu_{DC,rot}$  (Fig. 6) start to increase and decrease, respectively. Weakening dependence of  $W(f)$  on CoO is observed on approaching the MHz range. The dw processes tend to earlier relaxation compared to rotations (see Fig. 5) and the rotational losses become prevalent. The quantitative theoretical treatment of the latter, based on the application of Eq. (1), using the real and imaginary rotational permeability components as solution of the Landau-Lifshitz equation,<sup>12,17,18</sup> actually predicts that all

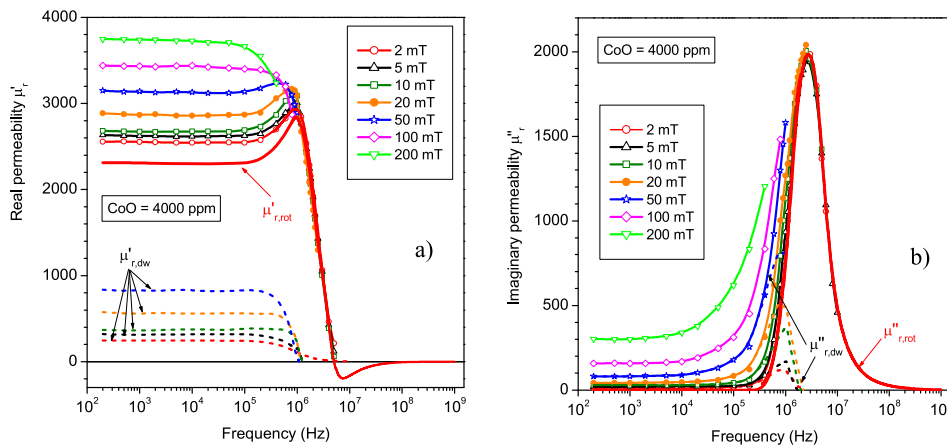


FIG. 5. Real  $\mu'$  (a) and imaginary  $\mu''$  (b) permeability components in the 4000 ppm CoO-doped Mn-Zn ferrites measured up to 1 GHz for  $J_p = 2 - 200$  mT and their decomposition into rotational and dw components. A unique  $\mu'_{rot}(f)$  and  $\mu''_{rot}(f)$  dependence with resonant response (continuous lines) is singled out up to about  $J_p = 50$  mT. The dashed lines show the calculated  $\mu'_{dw}(J_p, f)$  and  $\mu''_{dw}(J_p, f)$  curves. The initial permeability (i.e., at  $J_p = 2$  mT) is almost completely associated with the rotational process.

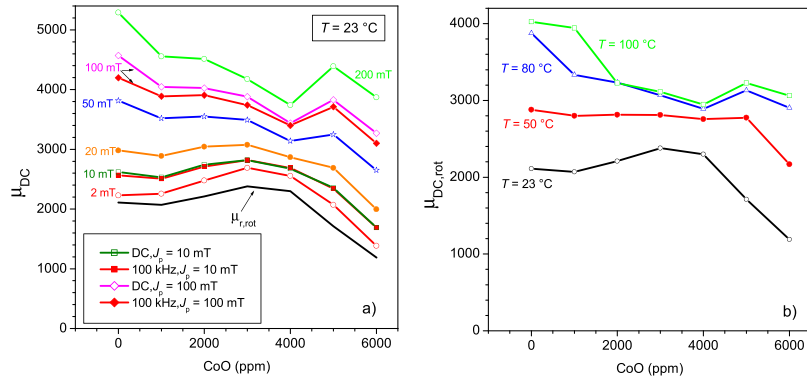


FIG. 6. a) Measured DC permeability  $\mu_{DC}$  at room temperature as a function of the CoO content at different induction levels ( $2\text{ mT} \leq J_p \leq 200\text{ mT}$ ).  $\mu_{DC}$  passes through a maximum value around  $\text{CoO} = 3000 - 4000\text{ ppm}$  at low  $J_p$  values, while it tends to decrease more or less monotonically beyond about  $20\text{ mT}$ . A small difference between  $\mu_{DC}$  and  $\mu(100\text{ kHz})$  can be appreciated only at the highest  $J_p$  values. The continuous line shows the behavior of the rotational contribution  $\mu_{DC,rot}$ , singled out according to the procedure sketched in Fig. 5a. This quantity well approximates the initial permeability (that is, in the limit  $H \rightarrow 0$ ). b) Dependence of the rotational (initial) permeability on the CoO content at different temperatures. A greater stability of the initial permeability versus temperature is obtained for  $\text{CoO} = 3000 - 4000\text{ ppm}$ .

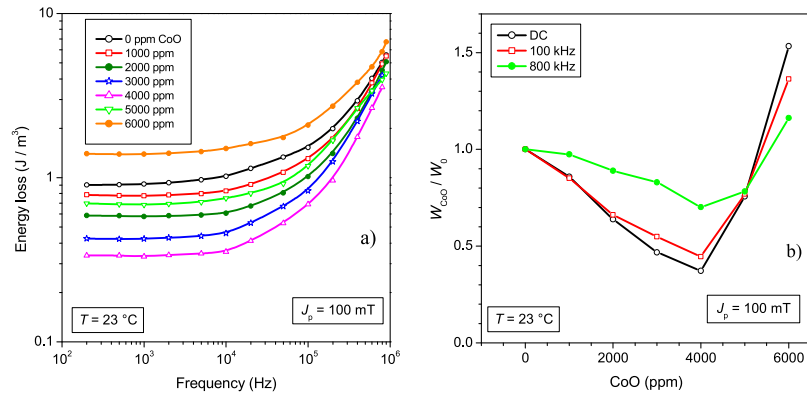


FIG. 7. a) Energy loss measured at  $J_p = 100\text{ mT}$  up to  $800\text{ kHz}$  in the Mn-Zn ferrites with different CoO content. b) The energy loss, here normalized with respect to the undoped sample, attains minimum value around  $3000 - 4000\text{ ppm}$ . Its dependence on the CoO content tends to weaken at high frequencies, because an increased proportion of the magnetization reversal is accomplished by rotations.

loss versus frequency curves eventually coalesce, for a given  $J_p$  value, on going deep into the MHz range.

## B. Effect of doping on the anisotropy. Temperature dependence of loss and permeability

Experimental knowledge of the rotational permeability permits one to obtain good insight on behavior and role of the magnetic anisotropy, whose manipulation is one key objective of doping. If we assume, in fact, that in the polycrystalline specimen the easy axes are uniformly distributed in the half-space and if we denote with  $K$  the average anisotropy constant, including the effects of the local demagnetizing fields, we estimate, with reasonable approximation, the DC relative rotational permeability of the ferrite sample as

$$\mu_{DC,rot} = 1 + \frac{J_s^2}{3\mu_0 K} \quad (2)$$

and we obtain the  $K$  (conventionally taken as positive) versus the CoO content shown in Fig. 8. It is generally assumed that by doping one might ideally achieve near-zero anisotropy, the result of compensation of the negative anisotropy of the host by the positive anisotropy of the added cations.

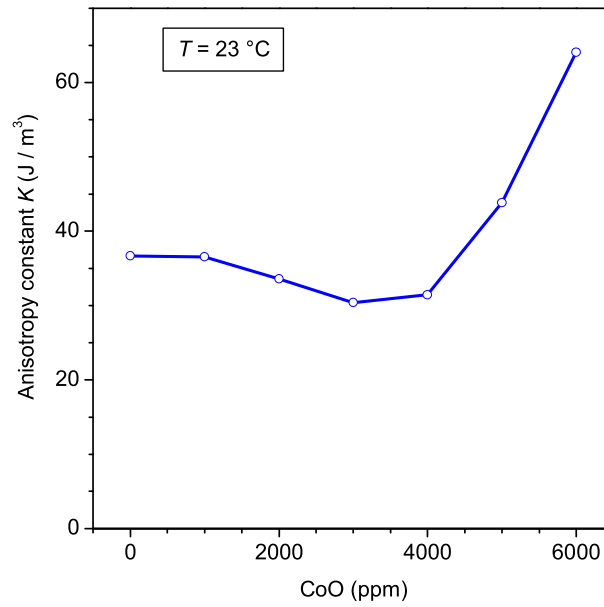


FIG. 8. The calculated anisotropy constant at room temperature attains minimum value around 3000-4000 ppm CoO.

The temperature at which full compensation expectedly occurs, with ideal passage of  $K$  through zero value and ensuing benefits in terms of increased permeability and lowered losses, is a function of the dopant concentration, which can be adjusted in order to achieve the best material response at a convenient temperature. Regarding the specific case of CoO doping, the temperature  $T$  at which minimum losses and maximum initial permeability are measured is generally found to decrease with increasing CoO content.<sup>9,10</sup> An example of energy loss dependence on temperature in the present materials is shown in Fig. 9, concerning a typical working condition, where  $J_p = 100$  mT and  $f = 100$  kHz. It is found that  $W(f)$  attains a minimum value between 80 °C and 100 °C, but for  $c_{Co} = 4000$  ppm. For this doping amount, providing minimum loss at room temperature (Fig. 9b), we obtain the greatest thermal stability of  $W(f)$  beyond room temperature. Anisotropy evolution with CoO and temperature is necessarily involved in such a behaviour, in combination with structural effects (pinning centers, grain boundaries, porosity). This is qualitatively recognized in the literature, but quantitative information is lacking. By singling out the rotational permeability  $\mu_{DC,rot}$ , as shown in Fig. 5, and by determining the saturation polarization  $J_s$  as a function of temperature, as shown in Fig. 10, we can estimate, by means of Eq. (2), the doping-dependent magnetic anisotropy  $K(T)$ . The temperature

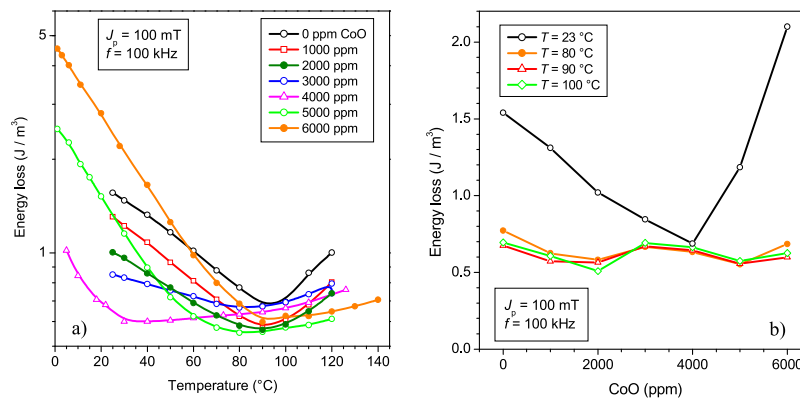


FIG. 9. a) Energy loss measured at  $J_p = 100$  mT and  $f = 100$  kHz as a function of temperature. b) The spread of  $W(f)$  values observed at room temperature shrinks upon attaining the optimal working temperatures of 80 °C – 100 °C.

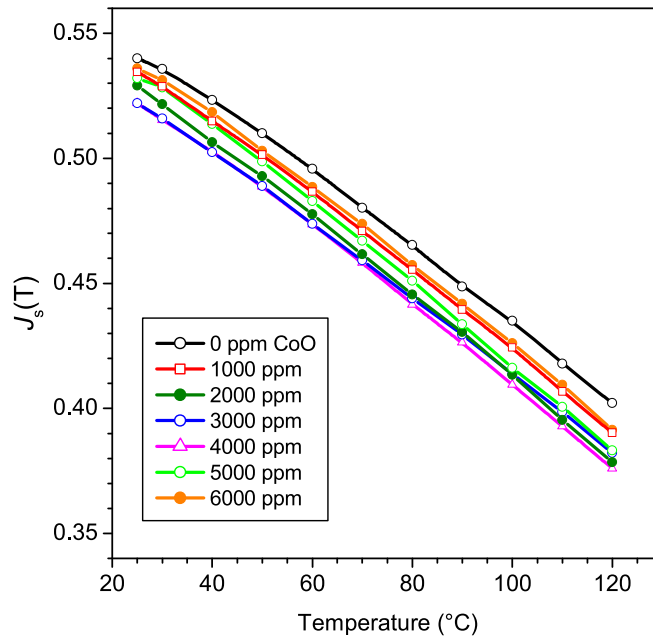


FIG. 10. Saturation polarization versus temperature in the CoO doped Mn-Zn ferrites.

dependence of  $\mu_{DC,rot}$  is shown in Fig. 11. It is noted that the secondary maximum of  $\mu_{DC,rot}$  versus temperature, usually assumed as due to the passage of  $K(T)$  through zero value, can be better understood, according to Eq. (2), in terms of competing decreasing behaviors of  $J_s$  and  $K$  with the temperature. We find in fact that  $K(T)$  is a CoO dependent monotonically decreasing function of temperature, as shown in Fig. 12. By taking then the difference between the calculated anisotropy constants for doped and undoped ferrites, we obtain the behavior of the additional term introduced by the  $Co^{2+}$  ions  $K_{Co}(T) = K(c_{Co}, T) - K(c_{Co}=0, T)$ . This is shown in Fig. 13. One can then conclude that CoO doping can provide, in agreement with the previously shown permeability and loss results, anisotropy compensation only below  $c_{Co} = 5000$  ppm and temperatures lower than about 60 °C.

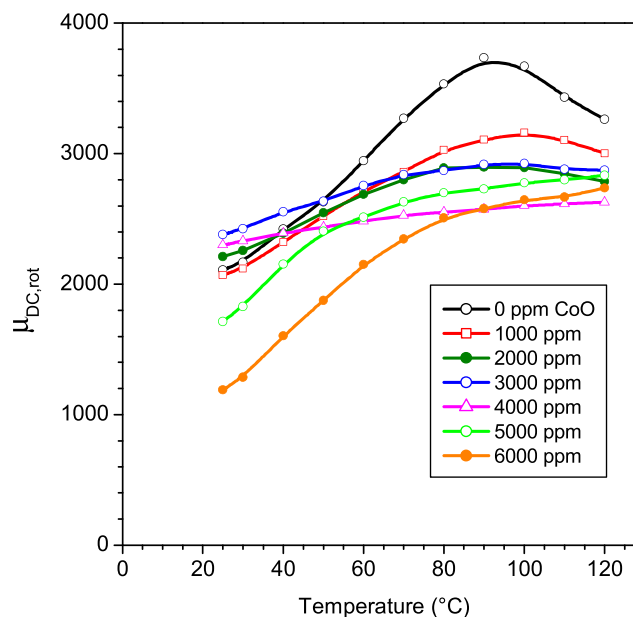


FIG. 11. Relative rotational permeability versus temperature as a function of CoO content.

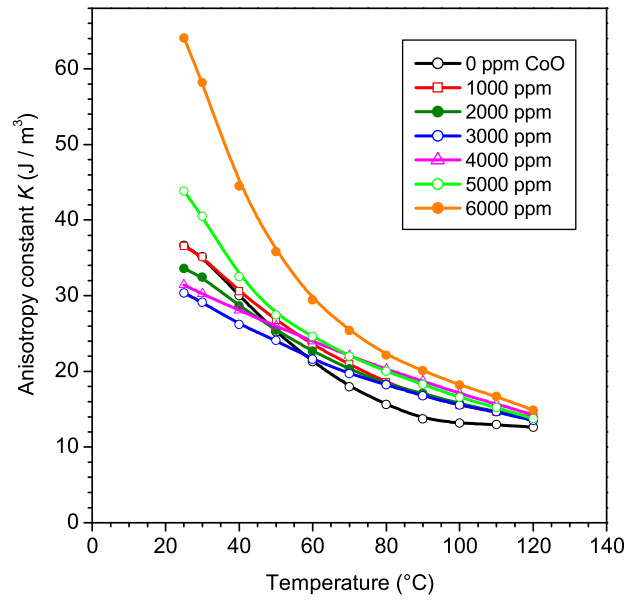


FIG. 12. Predicted behavior versus temperature of the magnetic anisotropy of the CoO doped Mn-Zn ferrites.

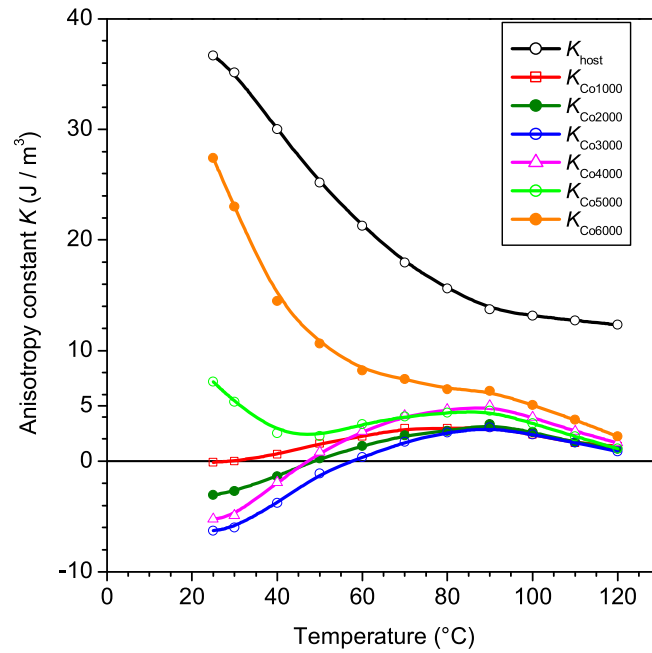


FIG. 13. The magnetic anisotropy of the undoped ferrite (conventionally taken as positive) is compared with the additional anisotropy introduced by the  $\text{Co}^{2+}$  ions. The mechanism of anisotropy compensation apparently operates below about 60 °C and  $c_{\text{Co}} < 5000$  ppm.

#### IV. CONCLUSIONS

A broadband investigation of permeability and loss behavior of sintered CoO-doped Mn-Zn ferrites has been made as a function of CoO content (up to  $c_{\text{Co}} = 6000$  ppm), peak polarization, and temperature. Magnetic softening by CoO addition, namely increase of the initial permeability and decrease of the magnetic losses, is observed to occur at room temperature for  $c_{\text{Co}} < \sim 5000$  ppm. The advantage of doping is observed, however, to weaken beyond a few hundred kHz and with increasing temperatures. It is in any case observed that the resistivity change brought about by

doping can interfere with the magnetic losses only at high frequencies, beyond a few MHz. By detailed analysis as a function of frequency, the complex permeability can be decomposed into dw and rotational contributions, with the latter directly linked, via additional knowledge of the saturation magnetization and its dependence on temperature, to the magnetic anisotropy. Assuming then isotropic distribution of the easy axes, the average effective magnetic anisotropy  $K$  has been estimated as a function of doping and temperature.  $K$ , conventionally taken positive in the host lattice, is always found to decrease monotonically with the temperature, with a trend depending on the CoO concentration. We thus find in the undoped sample  $K = 36.7 \text{ J/m}^3$  at room temperature, decreasing to  $K = 12.6 \text{ J/m}^3$  at  $T = 120^\circ\text{C}$ . All the  $K(T)$  curves belonging to different  $c_{\text{Co}}$  values actually tend to converge at such temperature, with minimum and maximum values  $K = 30.4 \text{ J/m}^3$  and  $K = 64.1 \text{ J/m}^3$  associated with  $c_{\text{Co}} = 3000 \text{ ppm}$  and  $c_{\text{Co}} = 6000 \text{ ppm}$ , respectively, at room temperature. We thus obtain that the contribution  $K_{\text{Co}}(T)$  from the foreign  $\text{Co}^{2+}$  ions subtracts from the anisotropy of the host lattice only below  $T \sim 60^\circ\text{C}$ , crossing the zero value for  $c_{\text{Co}}$  approaching 5000 ppm and eventually tending to disappear for  $T > 120^\circ\text{C}$ .

## ACKNOWLEDGMENTS

This work was performed in the context of the Agreement of Scientific and Technological Cooperation between INRIM and CERTH regarding the study of soft ferrites.

- <sup>1</sup> H. Shokrollahi and K. Janghorban, "Influence of additives on the magnetic properties, microstructure and densification of Mn-Zn soft ferrites," *Mater. Sci. Eng. B* **141**, 91–107 (2007).
- <sup>2</sup> S. Wang, Y. Chiang, Y. Hsu, and C. Chen, "Effects of additives on the loss characteristics of M-Zn ferrites," *J. Magn. Magn. Mater.* **365**, 119–125 (2014).
- <sup>3</sup> V. T. Zaspalis and E. Eleftheriou, "The effect of  $\text{TiO}_2$  on the magnetic power losses and electrical resistivity of polycrystalline MnZn ferrites," *J. Phys. D* **38**, 2156–2161 (2005).
- <sup>4</sup> K. Sun, Z. Lan, Z. Yu, L. Li, H. Ji, and Z. Xu, "Effects of NiO addition on the structural, microstructural and electromagnetic properties of manganese-zinc ferrite," *Mater. Chem. Phys.* **113**, 797–802 (2009).
- <sup>5</sup> B. Sun, F. Chen, W. Yang, H. Shen, and D. Xie, "Effects of nano- $\text{TiO}_2$  and normal size  $\text{TiO}_2$  additions on the microstructure and magnetic properties of manganese-zinc power ferrites," *J. Magn. Magn. Mater.* **349**, 180–187 (2014).
- <sup>6</sup> A. Znidarsic, M. Limpel, and M. Drofenik, "Effect of dopants on the magnetic properties of MnZn ferrites for high frequency power supplies," *IEEE Trans. Magn.* **31**, 950–953 (1995).
- <sup>7</sup> J. Hanuszkiewicz, D. Holz, E. Eleftheriou, and V. T. Zaspalis, "Materials processing issues influencing the frequency stability of the initial magnetic permeability of MnZn ferrites," *J. Appl. Phys.* **103**, 103907 (2008).
- <sup>8</sup> W. D. Yang and Y. G. Wang, "Effects of  $\text{TiO}_2$  and  $\text{Co}_2\text{O}_3$  combination additions on the elemental distribution and electromagnetic properties of Mn-Zn power ferrites," *J. Magn. Magn. Mater.* **384**, 13–17 (2015).
- <sup>9</sup> L. Li, Z. Lan, Z. Yu, K. Sun, and Z. Xu, "Effects of Co-substitution on wide temperature ranging characteristic of electromagnetic properties in MnZn ferrites," *J. Alloys Comp.* **476**, 755–759 (2009).
- <sup>10</sup> V. Tsakaloudi and V. Zaspalis, "Synthesis of a low loss Mn-Zn ferrite for power applications," *J. Magn. Magn. Mater.* **400**, 307–310 (2016).
- <sup>11</sup> H. Pascard, "Basic concepts for high permeability in soft ferrites," *J. Phys IV (France)* **8**(Pr2), 377–384 (1998).
- <sup>12</sup> F. Fiorillo and C. Beatrice, "A comprehensive approach to broadband characterization of soft ferrites," *Int. J. Appl. Electr. Mech.* **48**, 283–294 (2015).
- <sup>13</sup> F. Fiorillo, *Measurement and Characterization of Magnetic Materials* (Academic-Elsevier, San Diego CA, 2004) p. 409.
- <sup>14</sup> A. Caprile, M. Coisson, F. Fiorillo, P. Kabos, O. M. Manu, E. S. Olivetti, M. A. Olariu, M. Pasquale, and V. A. Scarlatache, "Microwave behavior of polymer bonded iron oxide nanoparticles," *IEEE Trans. Magn.* **48**, 3394–3397 (2012).
- <sup>15</sup> F. Fiorillo, C. Beatrice, M. Coisson, and L. Zhemchuzhna, "Loss and permeability dependence on temperature in soft ferrites," *IEEE Trans. Magn.* **45**, 4242–4245 (2009).
- <sup>16</sup> A. Fujita and S. Gotoh, "Temperature dependence of core loss in Co-substituted MnZn ferrites," *J. Appl. Phys.* **93**, 7477–7479 (2003).
- <sup>17</sup> F. Fiorillo, C. Beatrice, O. Bottauscio, and E. Carmi, "Eddy current losses in Mn-Zn ferrites," *IEEE Trans. Magn.* **50**, 6300109 (2014).
- <sup>18</sup> C. Beatrice, V. Tsakaloudi, S. Dobák, V. Zaspalis, and F. Fiorillo, "Magnetic losses versus sintering treatment in Mn-Zn ferrites," *J. Magn. Magn. Mater.* **429**, 129–137 (2017).
- <sup>19</sup> G. Bertotti, "Physical interpretation of eddy current losses in ferromagnetic materials," *J. Appl. Phys.* **57**, 2110–2117 (1985); *ibid.* **57**, 2118–2126 (1985).
- <sup>20</sup> J. F. Dillon, Jr. and H. E. Earl, Jr., "Domain wall motion and ferrimagnetic resonance in a manganese ferrite," *J. Appl. Phys.* **30**, 202–213 (1959).